Inorganic Chemistry

pubs.acs.org/IC Article

B-Site-Tuned Curie Temperature and Band Gap in Half-Metallic $LaCu_3B_2Re_2O_{12}$ (*B* = Fe, Co, Ni) Quadruple Perovskite Oxides

Shuai Tang, Zhehong Liu, Alexey V. Ushakov, Fedor Temnikov, Xubin Ye, Zhao Pan, Chien-Te Chen, Chang-Yang Kuo, Zhiwei Hu, Sergey V. Streltsov,* and Youwen Long*

Cite This: *Inorg. Chem.* 2026, 65, 3491−3497 Read Online

ACCESS | Metrics & More | Article Recommendations | Supporting Information

ABSTRACT: An *A*- and *B*-site-ordered quadruple perovskite oxide $LaCu_3Ni_2Re_2O_{12}$ was synthesized at 9 GPa and 1323 K. The crystal structure adopts a cubic space group of *Pn*-3 with the lattice constant $a = 7.4961(1)$ Å. Bond valence sum calculation and X-ray absorption spectroscopy suggest the charge distribution to be $La^{3+}Cu^{2+}{}_3Ni^{2+}{}_2Re^{5.5+}{}_2O_{12}$. A ferrimagnetic transition arising from the $Cu^{2+}(\uparrow)$-$Ni^{2+}(\uparrow)$-$Re^{5.5+}(\downarrow)$ spin coupling is found to occur at a Curie temperature of $T_C \approx 210$ K. First-principles calculations suggest a half-metallic electronic band structure for $LaCu_3Ni_2Re_2O_{12}$ with an energy gap of about 1.9 eV at the up-spin channel and a conducting band at the down-spin channel. By comparison with other isostructural $LaCu_3B_2Re_2O_{12}$ (*B* = Fe, Co, Ni) perovskites, we find that the electronic configuration of Re dominates the Curie temperature, as well as the half-metallic band gap.

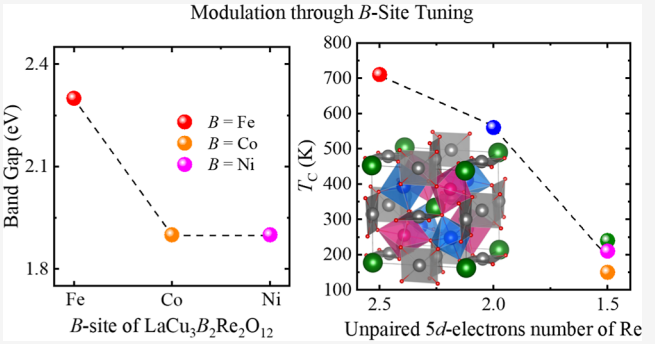

1. INTRODUCTION

Magnetic half-metals are distinguished by their intrinsically spin-polarized electronic structure, with one spin channel metallic and the other insulating or semiconducting, yielding complete spin polarization at the Fermi level in principle.[1−4] This property makes them promising candidates for spintronic applications such as magnetic storage, magnetoresistive sensors, energy-efficient electronics, quantum computing, etc.[3−8] Both *A*- and *B*-site-ordered quadruple perovskite oxides with the chemical formula $AA'_3B_2B'_2O_{12}$ provide an intriguing platform for studying high-performance half-metals.[9−15] In such an ordered structure, the *A*′, *B*, and *B*′ sites can all accommodate magnetic transition-metal ions, giving rise to multiple magnetic and electronic interaction pathways between *A*′-*B*, *A*′-*B*′, and *B*-*B*′ pairs. As a result, a wide variety of interesting physical properties like charge transfer, charge disproportionation, magnetoelectric multiferroicity, negative thermal expansion, and superior catalytic activity are found to occur.[16−22] Particularly, $CaCu_3Fe_2Re_2O_{12}$ was reported to possess a half-metallic band structure with a Curie temperature of $T_C \approx 560$ K.[10] By using La to replace Ca, a record high $T_C \approx 710$ K was observed in the $LaCu_3Fe_2Re_2O_{12}$ half-metal.[13] If the *A*-site is substituted by a monovalent ion of Na, however, one finds that the Curie temperature sharply decreases to about 240 K.[23] These results demonstrate the significant *A*-site tuning for the spin interactions in the $ACu_3Fe_2Re_2O_{12}$ family.[23] In comparison, a systematic study of *B*-site tuning for the $LaCu_3B_2Re_2O_{12}$ (*B* = 3*d* transition-metal ions) series remains limited. Our previous report shows that the Co occupancy at the *B*-site can also remarkably change the Curie temperature.[12] In this work, we report the high-pressure synthesis of novel *A*- and *B*-site-ordered quadruple perovskite oxide $LaCu_3Ni_2Re_2O_{12}$ (LCNRO). The crystal structure, charge state, magnetic and electrical transport properties, as well as the electronic properties are studied in detail. Moreover, the *B*-site substitution effects on magnetic and electronic properties are discussed for the half-metallic $LaCu_3B_2Re_2O_{12}$ (*B* = Fe, Co, or Ni) family.

2. EXPERIMENTAL AND CALCULATION SECTION

For complex perovskite oxides, ambient-pressure synthesis frequently results in phase segregation, oxygen nonstoichiometry, and destabilization of the target oxidation states (refer to Supporting Information Figure S1). High-pressure synthesis may mitigate these issues by stabilizing the dense perovskite structure, preserving the oxygen content, and promoting the desired *B*-site ordering. The bulk polycrystalline LCNRO was synthesized using highly pure (>99.9%) La_2O_3, CuO, NiO, ReO_2, and Re_2O_7 powders as starting materials. These reactants were well mixed with a stoichiometric mole ratio of 1:6:4:2:1 and sealed into a gold capsule after being ground thoroughly

Received: November 4, 2025
Revised: January 7, 2026
Accepted: January 26, 2026
Published: February 3, 2026

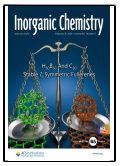

https://doi.org/10.1021/acs.inorgchem.5c05176
Inorg. Chem. 2026, 65, 3491−3497

in an agate mortar. Then the capsule was pressed on a cubic anvil-type high-pressure apparatus at 9 GPa and 1323 K for 30 min. After the heat treatment, pressure was gradually released to ambient pressure within 5 h. Then we peeled off the capsule to obtain a dense cylindrical sample. Synchrotron X-ray diffraction (SXRD) was performed on a finely ground powder sample using the beamline BL02B2 of SPring-8 in Japan with a wavelength λ = 0.42054 Å at room temperature (RT). Rietveld refinement was performed for the SXRD data using the GSAS program.[24] X-ray absorption spectroscopy (XAS) measurements at the Cu/Ni-L_3 edges were carried out in total-electron-yield mode at beamline TLS11A, and the Re-L_3 edge was measured in transmission mode at beamline TPS44A, both in the National Synchrotron Radiation Research Center (NSRRC) of Taiwan at RT. A specimen with a mass of 12.6 mg was cut from the sintered piece, and the magnetic susceptibility was measured between 2 and 350 K under an applied field of 0.1 T using a magnetic property measurement system (MPMS-VSM, Quantum Design) with field-cooled (FC) and zero-field-cooled (ZFC) modes. Isothermal magnetization curves were recorded at 2, 100, 200, and 300 K, respectively. The electrical resistivity was measured using a standard four-probe method on a sample cut and polished into a standard cuboid from the sintered piece, employing a Physical Property Measurement System (PPMS-9 T, Quantum Design). The specific heat was measured using a sample with a mass and thickness of approximately 12 mg and 1.3 mm, respectively, on the same PPMS.

The spin-polarized electronic structure theoretical calculations were carried out using the full-potential linearized augmented plane-wave (FP-LAPW) method as implemented in WIEN2K.[25] The convergence criteria are 0.000001 Ry for total energy and 0.000001 electrons for total charge. The crystallographic parameters obtained from the SXRD refinement were chosen as the starting parameters for optimization, and the atomic coordinates were relaxed until the interatomic forces fell below 0.5 mRy/Bohr. The generalized gradient approximation (GGA) and exchange−correlation functional in the Perdew−Burke−Ernzerhof (PBE) form were utilized.[26] We used a homogeneous grid of 1000 k-points over the Brillouin zone according to the Monkhorst−Pack scheme.[27] Muffin-tin radii were set to 1.96 au for Cu, 2.05 au for Ni, 1.92 au for Re, and 1.70 au for O. The plane-wave cutoff was determined by $R_{MT}K\max$ = 6.0. Strong Coulomb correlations are taken into account via the GGA + U approach.[28] The on-site Coulomb repulsion parameters were set to U = 8 eV for Cu, 6 eV for Ni, and 2 eV for Re, while the Hund's rule coupling parameters were set to J_H = 0.9 eV for Cu and Ni and 0.5 eV for Re.[29−31] The GGA + U calculations with spin−orbit coupling (SOC), which may be important for the 5d Re ions, were also carried out. However, the GGA + U + SOC results indicate that the inclusion of SOC does not affect the magnetic ground state and leads to negligible changes in the electronic structure obtained with the GGA + U method (refer to Supporting Information Figure S3). Subsequently, we only discuss the GGA + U results hereafter. The initial spin configuration in the LCNRO is collinear antiferromagnetic (AFM), with the Cu and Ni ions set to spin "up" and the Re ions set to spin "down".

3. RESULTS AND DISCUSSION

Figure 1 presents the SXRD pattern of LCNRO along with its Rietveld refinement results at RT. The diffraction data can be well fitted by both A- and B-site-ordered $AA'_3B_2B'_2O_{12}$-type quadruple perovskite structure models with the cubic space group Pn-3. The refined lattice parameter is a = 7.4961(1) Å. To assess the B-site ordering, the occupancy factors for A-site La and A'-site Cu were fixed at unity due to the large ionic size difference. Then, the ordering degree between the B-site Ni and B'-site Re was refined to be nearly 100% if the oxygen occupancy was constrained to be unity, considering the stoichiometric composition, as will be discussed later. The detailed refined structure parameters of the LCNRO are summarized in Table 1. Four of the Cu−O bonds are relatively short, suggesting the formation of the 4-fold square-planar

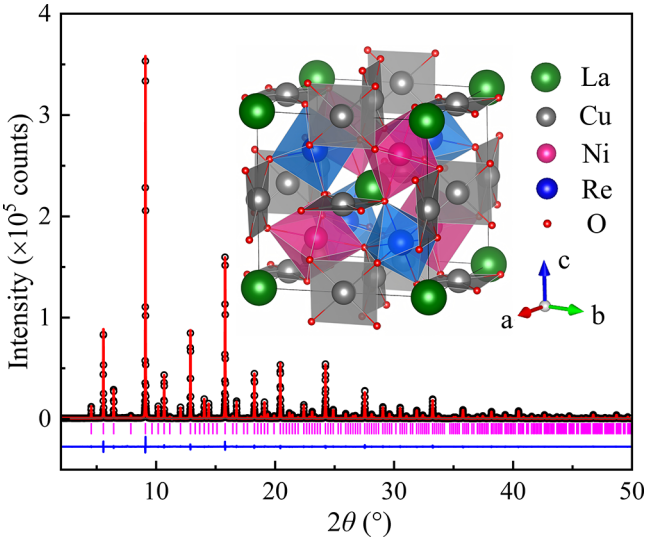

Figure 1. SXRD pattern and Rietveld refinement results for LCNRO at RT. The experimental (black circles), simulated (red line), and difference (blue line at the bottom) patterns are displayed. The Bragg reflection positions for space group Pn-3 are shown as magenta ticks. The inset illustrates the schematic crystal structure of LCNRO.

Table 1. Refined Structure Parameters of LCNRO at RT from SXRD Data[a]

site	WP	X	Y	Z	U_{iso} (100 × Å^2)
La	2*a*	0.25	0.25	0.25	0.98(3)
Cu	6*d*	0.25	0.75	0.75	0.58(1)
Ni	4*b*	0	0	0	0.56(6)
Re	4*c*	0.5	0.5	0.5	0.53(9)
O	24*h*	0.5734(2)	0.7595(3)	0.0549(9)	1.12(1)

bond length	value (Å)	bond angle	value (°)
Cu−O (×4)	1.977(4)	∠Ni−O−Re	139.79(9)
Ni−O (×6)	2.062(8)	∠Cu−O−Ni	107.03(8)
Re−O (×6)	1.931(7)	∠Cu−O−Re	112.41(9)
BVS (Cu)	2.01	BVS (Ni)	2.00

[a]Crystal data: space group Pn-3 (No. 201), a = 7.4961(1) Å. WP: Wyckoff position; R_{wp} = 4.67%, R_p = 3.46%. The formulas $V_i = \sum_j S_{ij}$ and $S_{ij} = \exp[(r_0 - r_{ij})/0.37]$ were used to calculate BVS values. The value of r_0 = 1.679 for Cu and 1.654 for Ni.

coordination of CuO_4 (see the inset of Figure 1). The corner-sharing Ni/ReO_6 octahedra are orderly arranged in a rock-salt-type manner and link with CuO_4 units by sharing O atoms. Based on the refined Cu−O and Ni−O bond lengths, the bond valence sum (BVS) calculations[32] suggest the presence of Cu^{2+} and Ni^{2+} (see Table 1). Meanwhile, compared with that of the Re-based perovskite oxides, the Re−O bond length of LCNRO (1.931 Å) is shorter than that of $Pb_2NiRe^{5+}O_6$ (1.979 Å in average)[33] and longer than that of $CaCu_3Co_2Re^{6+}{}_2O_{12}$ (1.892 Å),[34] implying the presence of an intermediate charge state between Re^{5+} and Re^{6+} in LCNRO, as revealed by the XAS measurement results shown below.

To validate the oxidation states in LCNRO, we performed XAS measurement, which is well known for its high element selectivity and sensitivity to the valence states and local coordination of transition metals.[35] Figure 2a,b shows the Cu- and Ni-L_3 edge spectra of LCNRO with references of CuO[36] and NiO,[37] respectively. The nearly identical energy positions between LCNRO and these references confirm the presence of

https://doi.org/10.1021/acs.inorgchem.5c05176
Inorg. Chem. 2026, 65, 3491−3497

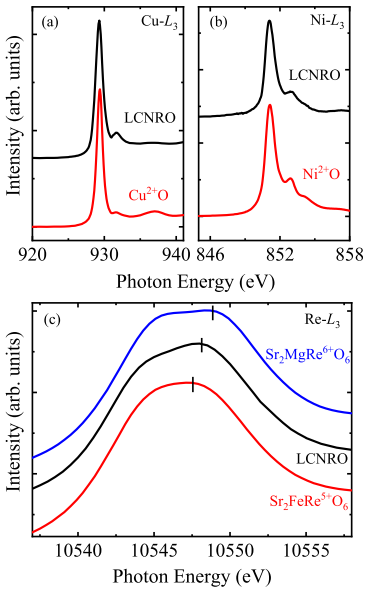

Figure 2. XAS spectra of (a) Cu-L_3 edge together with those of Cu^{2+} reference CuO, (b) Ni-L_3 edge together with those of Ni^{2+} reference NiO, and (c) Re-L_3 edge with Re^{6+} of Sr_2MgReO_6 and Re^{5+} of Sr_2FeReO_6 for LCNRO.

Cu^{2+} and Ni^{2+} valence states in LCNRO. Figure 2c presents the Re-L_3 edge XAS of LCNRO alongside those of $Sr_2MgRe^{6+}O_6$[38] and $Sr_2FeRe^{5+}O_6$[39] as the Re^{6+} and Re^{5+} references, respectively. Evidently, the energy position of LCNRO is located at the middle between these two references, indicating an average $Re^{5.5+}$ state in LCNRO, fulfilling the charge balance requirement. Therefore, these findings conclusively support the charge assignment of La-$Cu_3^{2+}Ni_2^{2+}Re_2^{5.5+}O_{12}$, which also confirms the stoichiometric chemical composition for LCNRO.

Figure 3a displays the temperature dependence of the magnetic susceptibility of LCNRO. As the temperature decreases, both ZFC and FC curves rise sharply at $T_C \approx 210$ K (determined by a tangent method as shown in Figure 3a), indicating a ferro- or ferrimagnetic phase transition. As shown in Figure 3b, the isothermal magnetization above T_C displays an almost linear behavior, which agrees with the paramagnetic state. At the temperatures below T_C, most clearly at 2 K, the magnetization loops exhibit typical magnetic hysteresis, which further indicates the ferro- or ferrimagnetic nature of LCNRO. Meanwhile, one finds that the saturated magnetic moment increases with decreasing temperature and reaches 5.0 μ_B/f.u. at 2 K and 7 T. Moreover, the coercive field of LCNRO is very small, with the value of only about 30 Oe at 2 K, as shown in the inset of Figure 3b, demonstrating the soft magnetic property. In the current LCNRO, the A'-site Cu^{2+}, B-site Ni^{2+}, and B'-site $Re^{5.5+}$ are all magnetic. If one considers the spin-only moment contribution, then both the collinear $Cu^{2+}(\uparrow)$-$Ni^{2+}(\uparrow)$-$Re^{5.5+}(\downarrow)$ and $Cu^{2+}(\uparrow)$-$Ni^{2+}(\downarrow)$-$Re^{5.5+}(\downarrow)$ ferrimagnetic coupling can generate the net spin moment (4.0 μ_B/f.u.) that is close to the experimental value (5.0 μ_B/f.u.). Based on the XMCD and neutron diffraction study, however, almost all the A- and B-site-ordered quadruple perovskite oxides exhibit $A'(\uparrow)$-$B(\uparrow)$-$B'(\downarrow)$-type ferrimagnetic coupling.[10−14,34,40−42] A similar ferrimagnetic alignment of $Cu^{2+}(\uparrow)$-$Ni^{2+}(\uparrow)$-$Re^{5.5+}(\downarrow)$ is thus temporarily assigned to the current LCNRO.

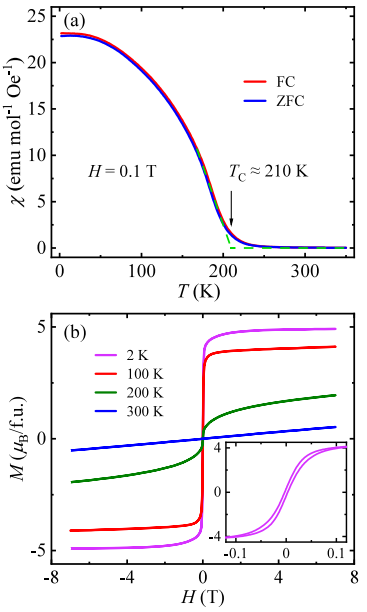

Figure 3. (a) Temperature-dependent magnetic susceptibility with ZFC and FC modes under 0.1 T for LCNRO. The green dashed lines are tangents to determine the T_C. (b) Magnetic field dependence of magnetization recorded at four selected temperatures for LCNRO. The inset shows the enlarged MH hysteresis at 2 K.

The temperature-dependent electrical resistivity of LCNRO is shown in Figure 4a. At 350 K, the resistivity value is about 0.16 Ω·cm. With decreasing temperature, the resistivity slightly increases to about 0.73 Ω·cm at 2 K without a visible anomaly occurring near T_C. Since grain boundary effects are inevitably involved in electrical transport measurement, the specific heat

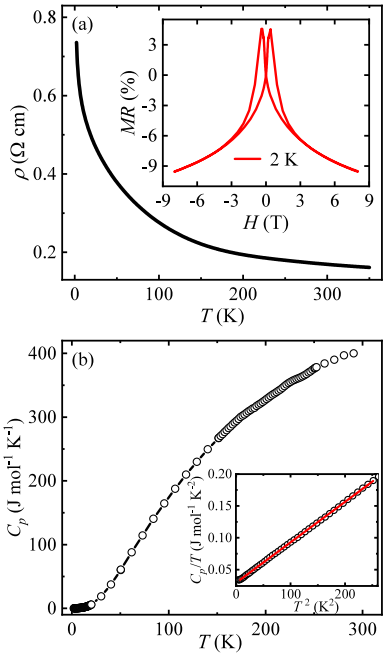

Figure 4. (a) Temperature dependence of electrical resistivity for LCNRO from 2 to 350 K measured at zero field. The inset depicts the field-dependent magnetoresistance effects measured at 2 K. (b) Temperature dependence of specific heat data for LCNRO from 2 to 290 K measured at zero field. The inset displays the fitting result (red line) based on the function $C_p/T = \gamma + \beta T^2$ from 2 to 16 K.

https://doi.org/10.1021/acs.inorgchem.5c05176
Inorg. Chem. 2026, 65, 3491−3497

of LCNRO was thus measured to further study the intrinsic transport properties. Figure 4b shows the specific heat data at 2−290 K for LCNRO. No remarkable anomaly is found to occur near the ferrimagnetic phase transition temperature, probably because most magnetic entropy has already been gradually released at temperatures higher than T_C. The low-temperature (<16 K) specific heat data can be well fitted using the function $C_p/T = \gamma + \beta T^2$, as shown in the inset of Figure 4b. The fitted Sommerfeld coefficient γ = 29.5(1) mJ·mol^{-1}·K^{-2}. Such a large γ value indicates the considerable contribution of electrons to specific heat, suggesting itinerant electronic states emerging near the Fermi level in LCNRO. Note that we also measured the Hall effects, and the results are consistent with an intrinsically metallic electronic structure with relatively weak/low carrier density (please refer to Supporting Information Figures S4 and S5). One thus believes that, intrinsically, LCNRO should exhibit metal-like electrical transport behavior, and the slight resistivity upturn with decreasing temperature observed in Figure 4a most probably originates from grain boundary effects due to the polycrystalline nature of the sample.[10−13] In addition, the inset of Figure 4a depicts the magnetoresistance (MR) effect [MR = 100% × (ρ(H)—ρ(0 T))/ρ(0 T)] of LCNRO as a function of magnetic field at 2 K. The MR curve exhibits a characteristic butterfly-like shape, indicative of spin-dependent tunneling behavior arising from spin-polarized conduction electrons through grain boundaries.[7,43,44] This behavior is consistent with observations of isostructural half-metallic perovskite oxides such as $LaCu_3Fe_2Re_2O_{12}$ and $LaCu_3Co_2Re_2O_{12}$.[12,13]

Spin-polarized electronic energy band structure calculations utilizing the DFT with electronic correlation effect (U) were carried out to analyze the electronic properties of LCNRO.[45] The theoretically calculated band structures and density of states (DOS) results are shown in Figure 5. An energy gap of

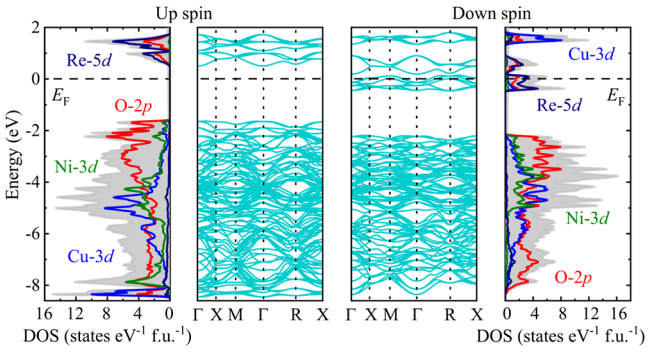

Figure 5. Calculated spin-polarized band structures and the DOS near the Fermi level (set to zero) of LCNRO using the GGA + U method with U = 8 eV for Cu, 6 eV for Ni, and 2 eV for Re, respectively. The total DOS (ashen shadow) and partial DOS of Cu-3d (blue line), Ni-3d (olive line), Re-5d (navy line), and O-2p (red line) are displayed, respectively.

approximately 1.9 eV in the up(majority)-spin bands is observed. However, the Fermi level crosses the down-(minority)-spin bands primarily composed of Re-5d states hybridized with O-2p and a few Cu-3d and Ni-3d states. Such an electronic structure is consistent with a half-metallic picture in which only one spin channel is conducting, while the other remains insulating. Furthermore, the 3d orbital electrons of Ni^{2+} predominantly occupy the up-spin bands, and Cu^{2+} 3d up-spin bands are almost fully filled, while the 5d electrons of $Re^{5.5+}$ are primarily found in the down-spin bands. This configuration aligns well with the Cu^{2+}(↑)-Ni^{2+}(↑)-$Re^{5.5+}$(↓) ferrimagnetic arrangement well.

If we compare the half-metallic $LaCu_3B_2Re_2O_{12}$ (B = Fe, Co, Ni) series, the calculated values of the band gap decrease with the B-site changing from Fe to Co while remaining almost unchanged from Co to Ni, as displayed in Figure 6a. This

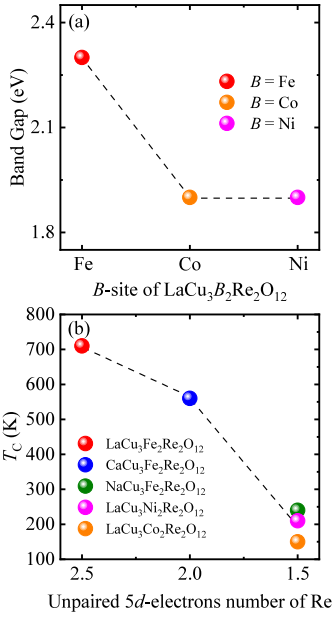

Figure 6. (a) DFT-calculated up(majority)-spin band gap of $LaCu_3B_2Re_2O_{12}$ as a function of B = Fe, Co, Ni. (b) Unpaired 5d-electron number of Re dependence of T_C for the $ACu_3B_2Re_2O_{12}$ (A = La, Ca, Na; B = Fe, Co, Ni) half-metal family.

tendency probably closely correlates with the number of unpaired Re-5d electrons. Energy splitting between the Re t_{2g} minority-spin and Re t_{2g} majority-spin states is defined by the intra-atomic Hund's exchange, which weakly depends on the Re valence state. Therefore, the band gap in the majority-spin channel is mostly defined by the charge transfer energy, which is the energy difference between ligand p and metal d states: $\Delta_{CT} = \varepsilon_d - \varepsilon_p$.[46] Going from Fe^{3+} to Co^{2+} (Ni^{2+}), the increased valence state of Re reduces Δ_{CT}[47,48] and, consequently, the band gaps—a result that aligns perfectly with our calculations. In contrast, changing Co^{2+} to Ni^{2+} does not modify the number of Re electrons, and the band gap stays almost the same. Therefore, one can achieve remarkable band gap modulation of this half-metallic quadruple perovskite family by changing the number of unpaired Re-5d electrons.

In addition, compared with $LaCu^{2+}{}_3Fe^{3+}{}_2Re^{4.5+}{}_2O_{12}$ ($T_C \approx$ 710 K), the B-site Ni substitution significantly reduces T_C by approximately 500 K,[13] bringing it close to that of $LaCu^{2+}{}_3Co^{2+}{}_2Re^{5.5+}{}_2O_{12}$ ($T_C \approx$ 150 K).[12] This modulation also arises primarily from changes in the number of unpaired Re-5d electrons: in this half-metal family, the Cu(↑)-B(↑)-Re(↓) ferrimagnetic order is dominated by antiferromagnetic superexchange along the Cu−Re and B-Re pathways, so fewer unpaired 5d electrons of Re can highly weaken the magnetic coupling[49] and thus suppress T_C. As shown in Figure 6b, A-site-substituted compounds $CaCu^{2+}{}_3Fe^{3+}{}_2Re^{5+}{}_2O_{12}$ ($T_C \approx$ 560 K)[10] and $NaCu^{2+}{}_3Fe^{3+}{}_2Re^{5.5+}{}_2O_{12}$ ($T_C \approx$ 240 K)[23] further demonstrate that tuning the Re unpaired electron number can

https://doi.org/10.1021/acs.inorgchem.5c05176
Inorg. Chem. 2026, 65, 3491−3497

substantially modulate T_C. In contrast, when the unpaired electron count of Re remains unchanged, T_C exhibits only minor variation, which may originate from structural factors such as *B*−O−Re bond angles, *B*-site ionic size, octahedral distortions, and/or metal−oxygen covalency. Therefore, achieving substantial T_C modulation through *B*-site substitution is fundamentally closely related to the alteration of the Re-5d unpaired electron number.

4. CONCLUSIONS

In summary, we synthesized a new *A*- and *B*-site-ordered quadruple perovskite oxide, $LaCu_3Ni_2Re_2O_{12}$, with the *Pn*-3 space group and a charge combination of $Cu^{2+}/Ni^{2+}/Re^{5.5+}$ using high-pressure and high-temperature methods. This material is a ferrimagnet with a T_C value of about 210 K. A saturated moment of 5.0 μ_B/f.u. and a small magnetic coercive field of less than 30 Oe at 2 K were observed. Theoretical calculations suggest that $LaCu_3Ni_2Re_2O_{12}$ has a half-metallic electronic band structure with completely spin-polarized conduction electrons in the minority-spin bands with an up-spin gap of 1.9 eV. *B*-site Ni substitution preserves the half-metallic character across the $LaCu_3B_2Re_2O_{12}$ (B = Fe, Co) family, while its pronounced effect on T_C and band gap arises from altering the number of unpaired Re-5d electrons. This work offers a clear case and guiding principles for designing and tuning the band gap and Curie temperature for half-metallic materials.

■ ASSOCIATED CONTENT

Supporting Information

The Supporting Information is available free of charge at https://pubs.acs.org/doi/10.1021/acs.inorgchem.5c05176.

Ambient-pressure synthesis, synthesis under different conditions, Hall effect measurements, carrier concentration analysis, and calculation details (PDF)

■ AUTHOR INFORMATION

Corresponding Authors

Sergey V. Streltsov − *Institute of Metal Physics, Ekaterinburg 620108, Russia;* orcid.org/0000-0002-2823-1754; Email: streltsov@imp.uran.ru

Youwen Long − *Beijing National Laboratory for Condensed Matter Physics, Institute of Physics, Chinese Academy of Sciences, Beijing 100190, China; School of Physical Sciences, University of Chinese Academy of Sciences, Beijing 100049, China;* orcid.org/0000-0002-8587-7818; Email: ywlong@iphy.ac.cn

Authors

Shuai Tang − *Beijing National Laboratory for Condensed Matter Physics, Institute of Physics, Chinese Academy of Sciences, Beijing 100190, China; School of Physical Sciences, University of Chinese Academy of Sciences, Beijing 100049, China;* orcid.org/0009-0008-5092-067X

Zhehong Liu − *Beijing National Laboratory for Condensed Matter Physics, Institute of Physics, Chinese Academy of Sciences, Beijing 100190, China*

Alexey V. Ushakov − *Institute of Metal Physics, Ekaterinburg 620108, Russia*

Fedor Temnikov − *Institute of Metal Physics, Ekaterinburg 620108, Russia*

Xubin Ye − *Beijing National Laboratory for Condensed Matter Physics, Institute of Physics, Chinese Academy of Sciences, Beijing 100190, China;* orcid.org/0000-0002-5739-8318

Zhao Pan − *Beijing National Laboratory for Condensed Matter Physics, Institute of Physics, Chinese Academy of Sciences, Beijing 100190, China;* orcid.org/0000-0002-8693-2508

Chien-Te Chen − *National Synchrotron Radiation Research Center, Hsinchu 30076, Taiwan*

Chang-Yang Kuo − *National Synchrotron Radiation Research Center, Hsinchu 30076, Taiwan; Department of Electrophysics, National Yang Ming Chiao Tung University, Hsinchu 30010, Taiwan*

Zhiwei Hu − *Max Planck Institute for Chemical Physics of Solids, Dresden 01187, Germany;* orcid.org/0000-0003-0324-2227

Complete contact information is available at: https://pubs.acs.org/10.1021/acs.inorgchem.5c05176

Notes

The authors declare no competing financial interest.

■ ACKNOWLEDGMENTS

This work was supported by the National Key R&D Program of China (Grant No. 2021YFA1400300), the National Natural Science Foundation of China (Grant Nos. 12261131499, 12425403, 12204516, and 12304268), and the China Postdoctoral Science Foundation (Grant No. 2023M743741). Theoretical DFT calculations were supported by the "Quantum" project (122021000038-7). Treatment of correlation effects by the DFT + *U* approach was supported by the Russian Science Foundation (grant RSF 23-42-00069). Dr. Zhiwei Hu acknowledges the support from the Max Planck-POSTECH-Hsinchu Center for Complex Phase Materials. The powder synchrotron X-ray diffraction experiments were performed at SPring-8 with the approval of the Japan Synchrotron Radiation Research Institute (2024A1506, 2024A1695, and 2025A1495).

■ REFERENCES

(1) Celotta, R.; Pierce, D. T. Polarized Electron Probes of Magnetic Surfaces. *Science* **1986**, *234*, 333.

(2) Zutic, I.; Fabian, J.; Das Sarma, S. Spintronics: Fundamentals and Applications. *Rev. Mod. Phys.* **2004**, *76*, 323.

(3) Katsnelson, M. I.; Irkhin, V. Y.; Chioncel, L.; Lichtenstein, A. I.; de Groot, R. A. Half-Metallic Ferromagnets: From Band Structure to Many-Body Effects. *Rev. Mod. Phys.* **2008**, *80*, 315.

(4) Fert, A. Nobel Lecture: Origin, Development, and Future of Spintronics. *Rev. Mod. Phys.* **2008**, *80*, 1517.

(5) De Groot, R. A.; Mueller, F. M.; Engen, P. G. V.; Buschow, K. H. J. New Class of Materials: Half-Metallic Ferromagnets. *Phys. Rev. Lett.* **1983**, *50*, 2024.

(6) Hwang, H. Y.; Cheong, S.-W. Enhanced Intergrain Tunneling Magnetoresistance in Half-Metallic CrO_2 Films. *Science* **1997**, *278*, 1607.

(7) Kobayashi, K.-I.; Kimura, T.; Sawada, H.; Terakura, K.; Tokura, Y. Room-Temperature Magnetoresistance in an Oxide Material with an Ordered Double-Perovskite Structure. *Nature* **1998**, *395*, 677.

(8) Felser, C.; Fecher, G. H.; Balke, B. Spintronics: A Challenge for Materials Science and Solid-State Chemistry. *Angew. Chem., Int. Ed.* **2007**, *46*, 668.

(9) Byeon, S.-H.; Lee, S.-S.; Parise, J. B.; Woodward, P. M.; Hur, N. H. New Ferrimagnetic Oxide $CaCu_3Cr_2Sb_2O_{12}$: High-Pressure

Synthesis, Structure, and Magnetic Properties. *Chem. Mater.* **2005**, *17*, 3552.
(10) Chen, W.; Mizumaki, M.; Seki, H.; Senn, M. S.; Saito, T.; Kan, D.; Attfield, J. P.; Shimakawa, Y. A Half-Metallic *A*- and *B*-Site-Ordered Quadruple Perovskite Oxide $CaCu_3Fe_2Re_2O_{12}$ with Large Magnetization and a High Transition Temperature. *Nat. Commun.* **2014**, *5*, 3909.
(11) Wang, X.; Liu, M.; Shen, X.; Liu, Z.; Hu, Z.; Chen, K.; Ohresser, P.; Nataf, L.; Baudelet, F.; Lin, H.-J.; Chen, C.-T.; Soo, Y.-L.; Yang, Y.; Jin, C.; Long, Y. High-Temperature Ferrimagnetic Half Metallicity with Wide Spin-up Energy Gap in $NaCu_3Fe_2Os_2O_{12}$. *Inorg. Chem.* **2019**, *58*, 320.
(12) Liu, Z.; Sun, Q.; Ye, X.; Wang, X.; Zhou, L.; Shen, X.; Chen, K.; Nataf, L.; Baudelet, F.; Agrestini, S.; Chen, C.-T.; Lin, H.-J.; Vasili, H. B.; Valvidares, M.; Hu, Z.; Yang, Y.; Long, Y. Quadruple Perovskite Oxide $LaCu_3Co_2Re_2O_{12}$: A Ferrimagnetic Half Metal with Nearly 100% *B*-Site Degree of Order. *Appl. Phys. Lett.* **2020**, *117*, 152402.
(13) Liu, Z.; Zhang, S.; Wang, X.; Ye, X.; Qin, S.; Shen, X.; Lu, D.; Dai, J.; Cao, Y.; Chen, K.; Radu, F.; Wu, W.-B.; Chen, C.-T.; Francoual, S.; Mardegan, J. R. L.; Leupold, O.; Tjeng, L. H.; Hu, Z.; Yang, Y.; Long, Y. Realization of a Half Metal with a Record-High Curie Temperature in Perovskite Oxides. *Adv. Mater.* **2022**, *34*, 2200626.
(14) Liu, Z.; Peng, J.; Wang, X.; Temnikov, F.; Ushakov, A.; Ye, X.; Pan, Z.; Zhang, J.; Pi, M.; Tang, S.; Chen, K.; Radu, F.; Hu, Z.; Chen, C.-T.; Chi, Z.; Pchelkina, Z.; Irkhin, V.; Shen, Y.; Streltsov, S. V.; Long, Y. High-Pressure Synthesis and High-Performance Half Metallicity of Quadruple Perovskite Oxide $DyCu_3Fe_2Re_2O_{12}$. *Fundam. Res.* **2024**.
(15) Wang, X.; Temnikov, F.; Ye, X.; Pi, M.; Pan, Z.; Li, W.; Hu, Z.; Chen, C.-T.; Kuo, C.-Y.; Dong, C.; Shen, Y.; Li, W.; Streltsov, S. V.; Long, Y. $CuCu_3Fe_2Os_2O_{12}$: A Room-Temperature Ferrimagnet with Reduced Thermal Conductivity. *Inorg. Chem.* **2025**, *64*, 20796.
(16) Long, Y.; Hayashi, N.; Saito, T.; Azuma, M.; Muranaka, S.; Shimakawa, Y. Temperature-Induced *A*−*B* Intersite Charge Transfer in an *A*-Site-Ordered $LaCu_3Fe_4O_{12}$ Perovskite. *Nature* **2009**, *458*, 60.
(17) Yamada, I.; Takata, K.; Hayashi, N.; Shinohara, S.; Azuma, M.; Mori, S.; Muranaka, S.; Shimakawa, Y.; Takano, M. A Perovskite Containing Quadrivalent Iron as a Charge-Disproportionated Ferrimagnet. *Angew. Chem.* **2008**, *120*, 7140.
(18) Wang, X.; Chai, Y.; Zhou, L.; Cao, H.; Cruz, C.; Yang, J.; Dai, J.; Yin, Y.; Yuan, Z.; Zhang, S.; Yu, R.; Azuma, M.; Shimakawa, Y.; Zhang, H.; Dong, S.; Sun, Y.; Jin, C.; Long, Y. Observation of Magnetoelectric Multiferroicity in a Cubic Perovskite System: $LaMn_3Cr_4O_{12}$. *Phys. Rev. Lett.* **2015**, *115*, 087601.
(19) Yamada, I.; Tsuchida, K.; Ohgushi, K.; Hayashi, N.; Kim, J.; Tsuji, N.; Takahashi, R.; Matsushita, M.; Nishiyama, N.; Inoue, T.; Irifune, T.; Kato, K.; Takata, M.; Takano, M. Giant Negative Thermal Expansion in the Iron Perovskite $SrCu_3Fe_4O_{12}$. *Angew. Chem., Int. Ed.* **2011**, *50*, 6579.
(20) Yagi, S.; Yamada, I.; Tsukasaki, H.; Seno, A.; Murakami, M.; Fujii, H.; Chen, H.; Umezawa, N.; Abe, H.; Nishiyama, N.; Mori, S. Covalency-Reinforced Oxygen Evolution Reaction Catalyst. *Nat. Commun.* **2015**, *6*, 8249.
(21) Wang, X.; Liu, Z.; Lu, D.; Pi, M.; Pan, Z.; Long, Y. *A*-Site Ordered Quadruple Perovskite Oxides: Structures, Properties and Prospects. *Chin. J. High Pressure Phys.* **2024**, *38*, 010101.
(22) Wang, X.; Ye, X.; Liu, Z.; Long, Y. High-Pressure Synthesis and Research Progress of Multi-Order Perovskite Oxides. *Chin. Sci. Bull.* **2025**, *70*, 3470.
(23) Zhang, J.; Temnikov, F.; Ye, X.; Wang, X.; Pan, Z.; Liu, Z.; Pi, M.; Tang, S.; Chen, C.-T.; Pao, C.-W.; Huang, W.-H.; Kuo, C.-Y.; Hu, Z.; Shen, Y.; Streltsov, S. V.; Long, Y. Large Manipulation of Ferrimagnetic Curie Temperature by *A*-Site Chemical Substitution in $ACu_3Fe_2Re_2O_{12}$ (*A* = Na, Ca, and La) Half Metals. *Inorg. Chem.* **2025**, *64*, 472.
(24) Rietveld, H. A Profile Refinement Method for Nuclear and Magnetic Structures. *J. Appl. Crystallogr.* **1969**, *2*, 65.
(25) Blaha, P.; Schwarz, K.; Tran, F.; Laskowski, R.; Madsen, G. K. H.; Marks, L. D. WIEN2k: An APW+lo Program for Calculating the Properties of Solids. *J. Chem. Phys.* **2020**, *152*, 074101.
(26) Perdew, J. P.; Burke, K.; Ernzerhof, M. Generalized Gradient Approximation Made Simple. *Phys. Rev. Lett.* **1996**, *77*, 3865.
(27) Monkhorst, H. J.; Pack, J. D. Special Points for Brillouin-Zone Integrations. *Phys. Rev. B:* **1976**, *13*, 5188.
(28) Dudarev, S.; Botton, G.; Savrasov, S.; Humphreys, C.; Sutton, A. Electron-Energy-Loss Spectra and the Structural Stability of Nickel Oxide: An LSDA+U Study. *Phys. Rev. B* **1998**, *57*, 1505.
(29) Sun, L.; Han, J.; Ge, Q.; Zhu, X.; Wang, H. Understanding the Role of Cu^+/Cu^0 Sites at Cu_2O Based Catalysts in Ethanol Production from CO_2 Electroreduction -A DFT Study. *RSC Adv.* **2022**, *12*, 19394.
(30) Been, E.; Lee, W.-S.; Hwang, H. Y.; Cui, Y.; Zaanen, J.; Devereaux, T.; Moritz, B.; Jia, C. Electronic Structure Trends Across the Rare-Earth Series in Superconducting Infinite-Layer Nickelates. *Phys. Rev. X* **2021**, *11*, 011050.
(31) Lim, T.-W.; Kim, S.-D.; Sung, K.-D.; Rhyim, Y.-M.; Jeen, H.; Yun, J.; Kim, K.-H.; Song, K.-M.; Lee, S.; Chung, S.-Y.; Choi, M.; Choi, S.-Y. Insights into Cationic Ordering in Re-Based Double Perovskite Oxides. *Sci. Rep.* **2016**, *6*, 19746.
(32) Brown, I.; Altermatt, D. Bond-Valence Parameters Obtained from a Systematic Analysis of the Inorganic Crystal Structure Database. *Acta Crystallogr.* **1985**, *41*, 244.
(33) Stoyanova-Lyubenova, T.; Dos santos-García, A. J.; Urones-Garrote, E.; Torralvo, M. J.; Alario-Franco, M. A. High-Pressure Synthesis, Structural and Complex Magnetic Properties of the Ordered Double Perovskite Pb_2NiReO_6. *Dalton Trans.* **2014**, *43*, 1117.
(34) Liu, Z.; Wang, X.; Ye, X.; Shen, X.; Bian, Y.; Ding, W.; Agrestini, S.; Liao, S.-C.; Lin, H.-J.; Chen, C.-T.; Weng, S.-C.; Chen, K.; Ohresser, P.; Nataf, L.; Baudelet, F.; Sheng, Z.; Francoual, S.; Mardegan, J. R. L.; Leupold, O.; Li, Z.; Xi, X.; Wang, W.; Tjeng, L. H.; Hu, Z.; Long, Y. Observation of *A*-Site Antiferromagnetic and *B*-Site Ferrimagnetic Orderings in the Quadruple Perovskite Oxide $CaCu_3Co_2Re_2O_{12}$. *Phys. Rev. B* **2021**, *103*, 014414.
(35) Burnus, T.; Hu, Z.; Wu, H.; Cezar, J. C.; Niitaka, S.; Takagi, H.; Chang, C. F.; Brookes, N. B.; Lin, H.-J.; Jang, L. Y.; Tanaka, A.; Liang, K. S.; Chen, C. T.; Tjeng, L. H. X-Ray Absorption and X-Ray Magnetic Dichroism Study on Ca_3CoRhO_6 and Ca_3FeRhO_6. *Phys. Rev. B* **2008**, *77*, 205111.
(36) Toyoda, T.; Masujima, T.; Shiwaku, H.; Ando, M. Hard X-Ray Absorption Spectroscopy of CuO and Cu_2O with a Photoacoustic Detector. *Appl. Phys. Lett.* **1991**, *59*, 3657.
(37) Jan, J.; Asokan, K.; Chiou, J.; Pong, W.; Tseng, P.; Chen, L.; Chen, F.; Lee, J.; Wu, J.; Lin, H.; Chen, C. X-Ray Absorption Spectroscopy Investigations on Oxidized Ni/Au Contacts to *p*-GaN. *J. Synchrotron Radiat.* **2001**, *8*, 827.
(38) Wiebe, C.; Greedan, J.; Kyriakou, P.; Luke, G.; Gardner, J.; Fukaya, A.; Gat-Malureanu, I.; Russo, P.; Savici, A.; Uemura, Y. Frustration-Driven Spin Freezing in the S = 1/2 fcc Perovskite Sr_2MgReO_6. *Phys. Rev. B* **2003**, *68*, 134410.
(39) Herrero-Martín, J.; Subías, G.; Blasco, J.; García, J.; Sánchez, M. X-Ray Absorption Spectroscopic Study on A_2FeReO_6 Double Perovskites. *J. Phys.: Condens. Matter* **2005**, *17*, 4963.
(40) Gao, L.; Wang, X.; Ye, X.; Wang, W.; Liu, Z.; Qin, S.; Hu, Z.; Lin, H.-J.; Weng, S.-C.; Chen, C.-T.; Ohresser, P.; Baudelet, F.; Yu, R.; Jin, C.; Long, Y. Near-Room-Temperature Ferrimagnetic Ordering in a *B*-Site-Disordered 3d−5d-Hybridized Quadruple Perovskite Oxide, $CaCu_3Mn_2Os_2O_{12}$. *Inorg. Chem.* **2019**, *58*, 15529.
(41) Wang, X.; Liu, Z.; Deng, H.; Agrestini, S.; Chen, K.; Lee, J.-F.; Lin, H.-J.; Chen, C.-T.; Choueikani, F.; Ohresser, P.; Wilhelm, F.; Rogalev, A.; Tjeng, L. H.; Hu, Z.; Long, Y. Comparative Study on the Magnetic and Transport Properties of *B*-Site Ordered and Disordered $CaCu_3Fe_2Os_2O_{12}$. *Inorg. Chem.* **2022**, *61*, 16929.
(42) Ye, X.; Yin, Y.; Cao, Y.; Liao, Z.; Wang, X.; Liu, M.; Wang, Q.; Pan, Z.; Hu, Z.; Lin, H.-J.; Chen, C. T.; Pao, C.-W.; Ohresser, P.; Nataf, L.; Baudelet, F.; Yang, W.; Yang, J.; Cheng, J.; Yu, P.; Qiu, X.;

https://doi.org/10.1021/acs.inorgchem.5c05176
Inorg. Chem. 2026, 65, 3491−3497

Yang, Y.; Xiang, T.; Long, Y. High-Temperature Ferrimagnetic Order Triggered Metal-to-Insulator Transition in $CaCu_3Ni_2Os_2O_{12}$. *Nat. Commun.* **2025**, *16*, 3746.
(43) Hwang, H.; Cheong, S.; Ong, N.; Batlogg, B. Spin-Polarized Intergrain Tunneling in $La_{2/3}Sr_{1/3}MnO_3$. *Phys. Rev. Lett.* **1996**, *77*, 2041.
(44) Coey, J. Powder Magnetoresistance (Invited). *J. Appl. Phys.* **1999**, *85*, 5576.
(45) Şaşıoğlu, E.; Sandratskii, L. M.; Bruno, P. First-Principles Calculation of the Intersublattice Exchange Interactions and Curie Temperatures of the Full Heusler Alloys Ni_2MnX (X = Ga, In, Sn, Sb). *Phys. Rev. B* **2004**, *70*, 024427.
(46) Zaanen, J.; Sawatzky, G. A.; Allen, J. W. Band Gaps and Electronic Structure of Transition-Metal Compounds. *Phys. Rev. Lett.* **1985**, *55*, 418.
(47) Ushakov, A. V.; Streltsov, S. V.; Khomskii, D. I. Crystal Field Splitting in Correlated Systems with Negative Charge-Transfer Gap. *J. Phys.: Condens. Matter* **2011**, *23*, 445601.
(48) Mizokawa, T. Electronic Structure of 5d Transition-Metal Compounds. *J. Electron Spectrosc. Relat. Phenom.* **2016**, *208*, 78.
(49) Temnikov, F.; Ushakov, A. V.; Komleva, E. V.; Liu, Z.; Long, Y.; Irkhin, V. Y.; Streltsov, S. V. Exchange interaction in $ACu_3Fe_2Re_2O_{12}$ quadruple perovskites. *Phys. Rev. B* **2025**, *112*, 224427.

https://doi.org/10.1021/acs.inorgchem.5c05176
Inorg. Chem. 2026, 65, 3491−3497